

Mechanism of Oleic Acid-Mediated Sulfur Vacancy Healing in monolayer WS₂

Leon Daniel, Dedi Sutarma, Osamah Kharsah, Charleen Lintz, Peter Kratzer,
and Marika Schleberger*

Faculty of Physics and CENIDE, University of Duisburg-Essen, Germany

E-mail: marika.schleberger@uni-due.de

Phone: +49 203 379 1600/1601. Fax: +49 203 379 2334

Abstract

We uncover the mechanism behind the enhancement of photoluminescence yield in monolayer WS₂ through oleic acid treatment, a promising scalable strategy for defect healing. By inducing sulfur vacancies through thermal treatment and monitoring the changes in photoluminescence yield and emission spectra, we demonstrate that oleic acid heals the sulfur vacancy by providing substitutional oxygen. Using density functional theory calculations, we provide insight into the underlying mechanism governing the oleic acid-mediated sulfur vacancy healing process. Our findings suggest that effective defect passivation by oxygen doping can be achieved through chemical treatment, opening a pathway for oxygen doping in transition metal dichalcogenides. However, we also highlight the limitations of chemical treatment, which may only lead to small increases in photoluminescence yield beyond a certain point.

Transition metal dichalcogenides (TMDCs), particularly tungsten disulfide (WS₂), are promising candidates for next-generation optoelectronic and valleytronic devices due to their unique two-dimensional (2D) nature and exceptional optoelectronic properties.^{1,2} As a direct

bandgap semiconductor, monolayer WS_2 has a bandgap of 2.4-2.7 eV,³⁻⁵ making it suitable for applications in the visible range.⁵⁻⁷ Its high photoluminescence (PL) yield⁸⁻¹⁰ enables a wide range of applications, from LEDs to photodetectors.^{11,12} To develop WS_2 -based applications, precise control and manipulation of defects, particularly vacancies, are essential. Vacancies can significantly affect the electronic structure of TMDCs and modify their optical and electronic properties, allowing for customization of device functionalities.¹³⁻¹⁹

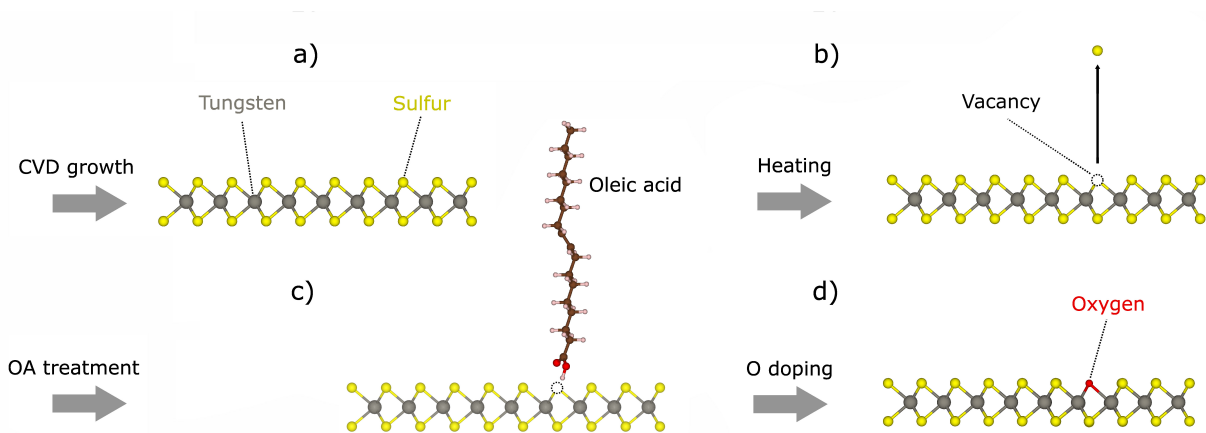


Figure 1: a) WS_2 grown by CVD is heated to introduce single vacancies (b). The defective material is then treated with oleic acid (c), which substitutes the vacancy with an oxygen atom (d).

Point defects in WS_2 , such as sulfur vacancies, introduce flat defect states in the bandgap, altering the material's native properties. These vacancies can act as a doping level or facilitate non-radiative recombination, affecting exciton recombination time and quantum efficiency (QE).^{17,20-22} To achieve specific material properties through defect engineering, both defect creation and passivation are crucial. Thermal treatment and ion irradiation have been used to induce vacancies in TMDCs, enabling precise control over defect type and density.^{18,23-28}

Vacancy healing, on the other hand, remains a significant challenge. Chemical treatments, such as super acid TFSI,²⁹⁻³¹ have been explored as an effective and scalable approach to restore vacancies and enhance performance. However, handling these chemicals can be difficult due to their corrosive nature.³² A benign-by-design chemistry is therefore desirable. Oleic

acid, a relatively weak acid and harmless alternative, has garnered significant interest due to its ability to effectively passivate vacancies in WS₂ and enhance photoluminescence properties by increasing the QE of TMDCs, while preserving their n-doping characteristics.^{33–36}

However, the exact mechanism of the healing remains unclear. Our goal is to assess the efficacy of oleic acid in restoring the material’s pristine characteristics and to reveal the underlying mechanism of the vacancy healing process. To this end, we used in-situ photoluminescence (PL) to analyze the evolution of vacancy density and band structure. By combining experiments on pristine and defective WS₂ with first-principles calculations, we found that oleic acid molecules act as an oxygen source, saturating sulfur vacancies in WS₂ and removing defect in-gap states, leading to improved PL (as schematically depicted in Figure 1). Our work thus demonstrates the feasibility and limits of using chemical treatments for defect management in WS₂, paving the way for optimized optoelectronic and valleytronic devices.

Our study begins with a characterization of pristine WS₂ samples grown by chemical vapor deposition (CVD, for details see Methods section). An optical microscopy image of a typical triangular monolayer flake is shown in Figure 2a) together with the integrated PL intensity map. Starting from the center, the PL intensity increases outwards, i.e. along the direction of growth of the flake. This is indicative of strong oxygen doping^{37,38} as we use no hydrogen to bind excess oxygen. The substitution of vacancies with oxygen enhances PL emission by removing in-gap defect states, enabling non-radiative recombination.^{21,22} This is in agreement with DFT calculations showing that a vacancy saturated with an oxygen atom is highly favorable (see Supplementary Information and^{21,22,37–39}).

All further measurements were conducted at the spot with a strong PL intensity, marked with a black circle in Figure 2a). Figure 2b) displays a recorded Raman spectrum of the monolayer. By using a 457 nm laser, the 2LA (*M*) mode at 350.4 cm⁻¹ is strongly suppressed, enabling a clear view on the E_{2g}¹ (Γ) mode at 356.8 cm⁻¹ and A_{1g} (Γ) mode at 416.9 cm⁻¹, confirming the monolayer.^{40–42}

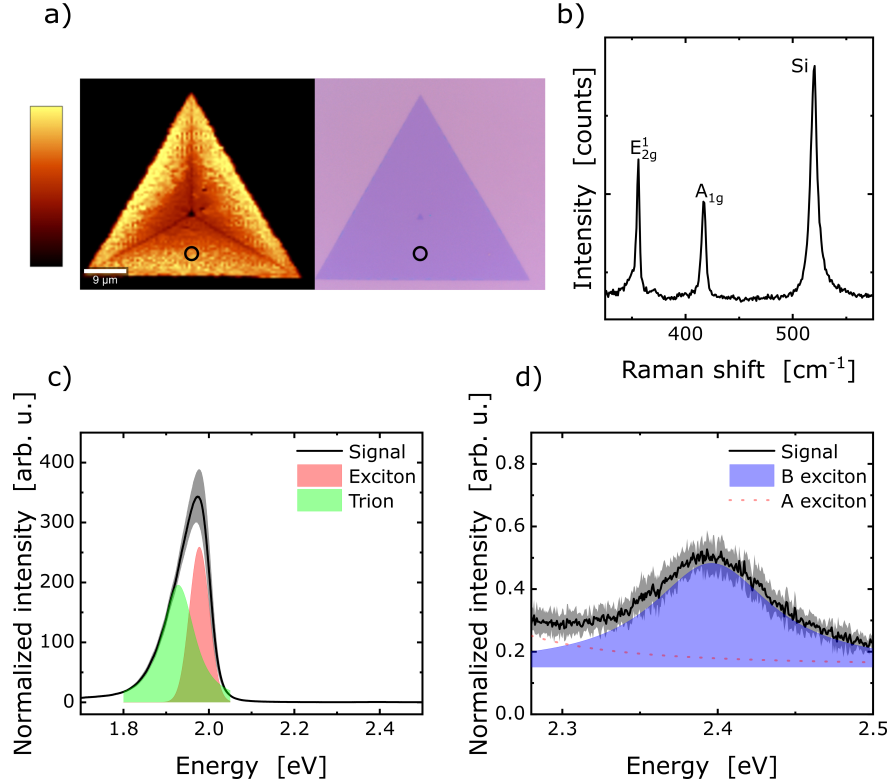


Figure 2: a) Microscope image of a monolayer WS₂ with corresponding PL map showing integrated intensity, with measurement locations marked. b) Raman spectra with assigned Raman modes. c) PL spectra of WS₂ monolayer from 1.7 to 2.5 eV measured at 80 K, with fitted trion and exciton peaks. d) Zoomed-in section of the PL spectrum, highlighting the smaller B exciton signal.

The pristine sample shows a strong emission at around 1.93 eV (Fig. 2c)), corresponding to the typical PL spectra for monolayer WS₂.^{2,6,7} The PL signal is comparable to that of an exfoliated reference sample, indicating a low intrinsic defect concentration. The peak is asymmetric, suggesting the presence of trions.⁴³

The zoomed-in section of the PL spectra in Figure 2d) features the less intensive B exciton. This is consistent with the literature, where the A exciton emission is about 1,800 times stronger than the B exciton emission.^{6,7} We modeled the band structure of a pristine WS₂ monolayer via DFT calculations. Our calculations show a valence band splitting of 430 meV, which is 16 times higher than the conduction band splitting of 28 meV, consistent with literature values.⁵⁻⁷ The predicted energy difference of the optical transition (402 meV) matches our experimental value of 420 meV ± 7 meV measured at 80 K very well.

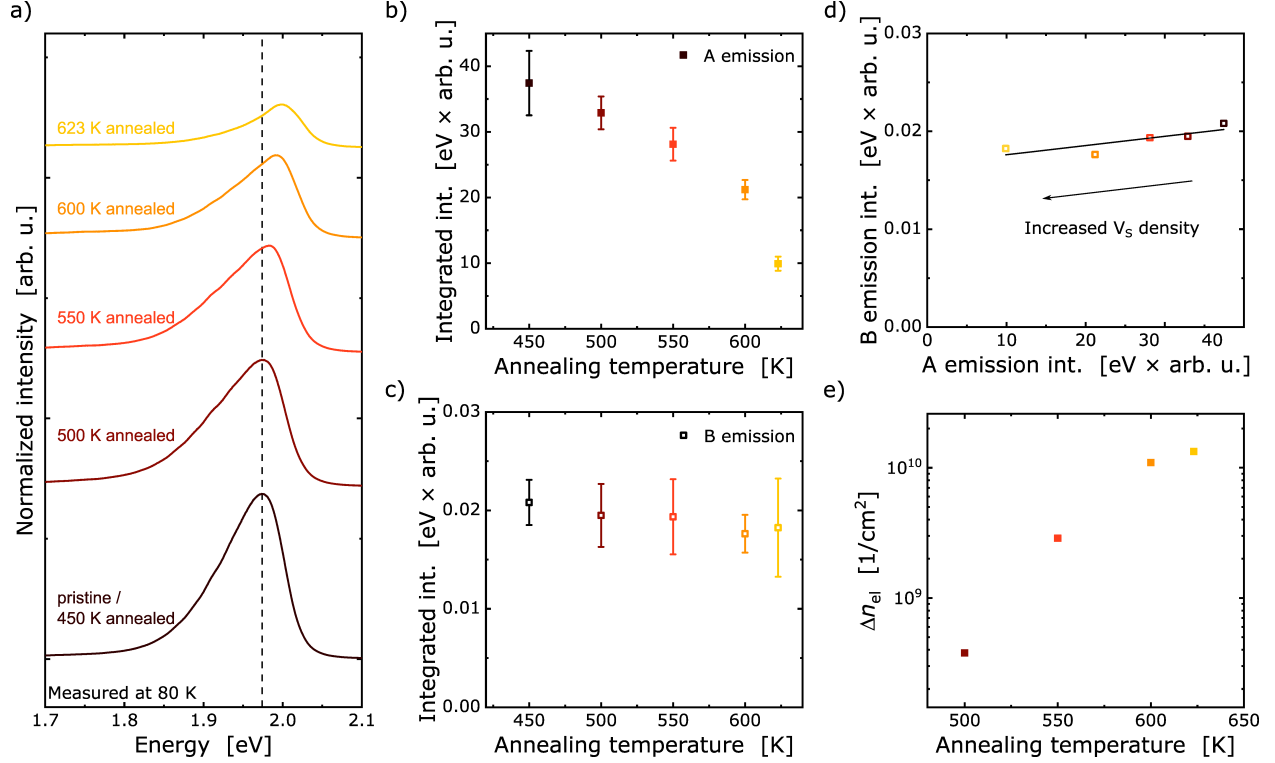


Figure 3: a) Normalized PL spectra of WS₂ for each heating step. b) and c) Signal intensity evolution of A and B emission with heating steps. d) B emission vs. A emission for the heated sample e) Evolution of free carrier density with increasing heating steps, calculated using the mass action model.

Next, we introduce sulfur vacancies by thermal processing, heating the sample to increasing temperatures and rapidly cooling to 80 K between each step (Methods section). In Figure 3a), the corresponding PL signal for the A-exciton is shown for selected temperature steps. The signal remains stable up to 450 K, consistent with other experiments.²⁷ However, with further temperature increase, the signal intensity decreases significantly, dropping to 26.5% of the original intensity at 623 K. This is attributed to an increase in sulfur vacancies, which enable non-radiative recombination and reduce bright emission.^{20,21} Supporting DFT calculations show that the formation energy for a sulfur vacancy is 2.72 eV, significantly lower than other types of vacancies. Additionally, the reaction enthalpy for sulfur removal in the presence of oxygen is -0.09 eV, indicating enhanced sulfur vacancy creation.

The B exciton, emitted by a different optical recombination path, shows no significant change in emission, as seen in Figure 3c). This suggests that the radiative recombination of

the B exciton is unaffected by defects that influence non-radiative recombination of the A exciton. The ratio between A exciton emission and B exciton emission is often associated with defect density. For example, ion irradiation in MoS2 has been shown to decrease A exciton emission relative to B exciton emission.¹³ McCreary et al. proposed a linear dependency of the intensity ratio of B and A emission in TMDCs: $I(B) = b + a \times I(A)$ with a and b positive constants determined from WS₂ samples with various defect densities.⁴⁴ we have plotted the intensity ratio of A and B exciton emission in Figure 3d). We determine $a = 0.00015 \pm 0.00005$, and from the intersection with the y-axis $b = 0.015 \pm 0.002$.

To check if the correlation between A and B excitons is universal or defect-type-dependent, we compared the correlation in a sample irradiated with different fluences of 100 eV argon ions, which increases in-gap states.⁴⁵ The correlation differs significantly, and can be described by $I(B) = 0.0006 + 0.024 \times I(A)$, see SI. This suggests that individual defects can be differentiated based on the type of correlation between A and B excitons. Additionally, increasing sulfur vacancies should decrease the A exciton signal to almost zero while only slightly affecting the B exciton, indicating no large conversion from B excitons to A excitons.

With increasing vacancy density, the emission peak becomes increasingly asymmetric, attributed to increased trion emission at higher heating temperatures (see SI). This is consistent with the law-of-mass-action model, which describes the correlation between free charge carrier density and trion emission in TMDCs.⁴⁶⁻⁵⁰

$$\frac{N_X n_{el}}{N_{X^-}} = \frac{4m_X m_e}{\pi \hbar^2 m_{X^-}} k_B T \exp\left(-\frac{E_b}{k_B T}\right) \quad (1)$$

N_X and N_{X^-} are the concentration of free excitons and trions, m_e , m_X and m_{X^-} are the effective mass of the electron, free exciton and trion, k_B and T are the Boltzmann constant and temperature, and E_b is the trion binding energy. We estimate the change in free charge carrier density Δn_{el} with higher heating steps, as shown in Figure 3e), which suggests a maximum increase of up to $1.3 \cdot 10^{10} \text{ cm}^{-2}$ for the final heating state. These carriers are attributed to ionized donor levels associated with S (or Se) vacancies.^{51,52}

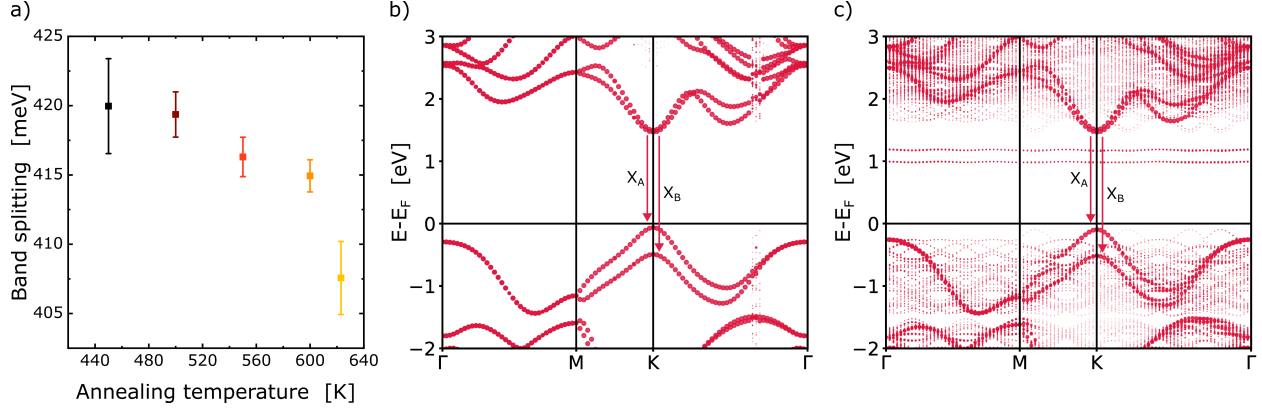


Figure 4: a) Valence band splitting with increasing treatment temperature, with error bars representing one standard deviation. Band structure of WS_2 in pristine condition (b) and with a V_S vacancy (c). The energetic difference between A and B emission (X_A and X_B) decreases by 20.1 meV.

The signal position is analyzed to determine the splitting of conduction and valence bands. A significant shift in the A exciton maxima is observed with increasing defect density, as seen in Figure 3a), while the B exciton remains largely unaffected. The A-B-exciton splitting is plotted for different heating steps in Figure 4a). The origin of the band splitting is the spin-orbit coupling (SOC) induced mostly by tungsten.^{53,54} Sulfur vacancies have inconclusive effects on the band structure. However, some studies associate them with a red-shift due to higher trion emission¹⁷ and DFT calculations suggest a slight increase in the band gap of WS_2 .²¹

We analyzed the electronic band structure of WS_2 with various defects (V_S , V_{WS_3} , O_S). The results for pristine WS_2 and V_S are shown in Figure 4b) and 4c). The vacancy induces two unoccupied states in the band gap and an occupied state in the valence band, leading to non-radiative recombination.⁵⁵ The calculations also suggest a decrease in the energetic difference between A and B emission of 20.1 meV, comparable to the experimental value. The removal of a WS_3 cluster or oxygen substitution have only negligible effects, see SI.

In the following, we examine the effect of oleic acid treatment on restoring the PL signal in defective samples. After thermal treatment, the PL intensity drops and shifts to the blue

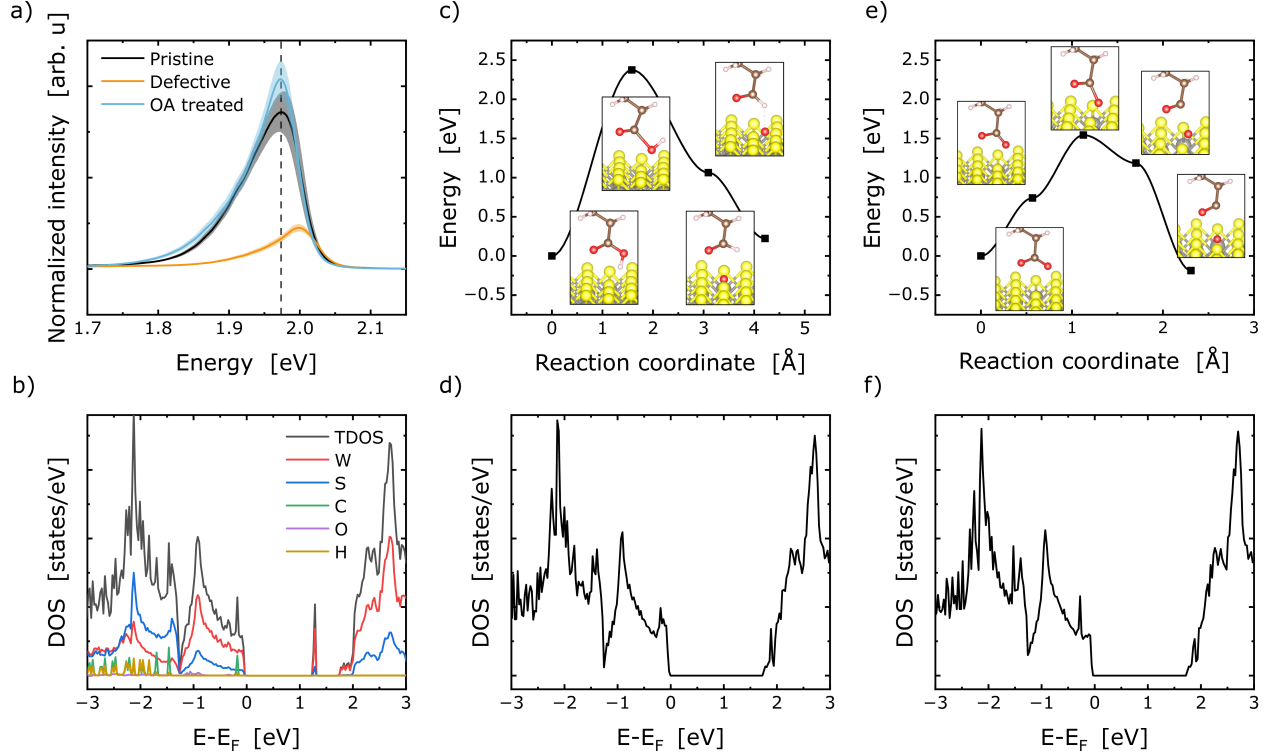


Figure 5: a) Normalized PL signal at 80 K of a pristine CVD-grown sample after heating to 623 K and subsequent oleic acid treatment. b) Element-resolved density of states (DOS) of oleic acid adsorbed on a sulfur vacancy in WS_2 . c) Reaction path of oleic acid with corresponding DOS (d) at the final reaction step. e) Reaction path of de-protonated oleic acid with corresponding DOS (f) at the final reaction step.

(Figure 5a). However, oleic acid treatment significantly increases the PL intensity, consistent with previous reports.^{33–36} The A exciton emission increases by a factor of 4 on average, while the B exciton emission increases by 19%. This is attributed to the elimination of defect-induced in-gap states. The recovered PL emission of the A exciton exceeds the pristine sample’s by 8%. This might be due to a step in the oleic acid treatment, which involves washing in toluene. This might reduce contaminations present on WS_2 , enhancing electron-hole recombination. We also observe a slight reduction in doping concentration by up to $1.12 \times 10^{10} \text{ cm}^{-2}$ and a shift in A emission spectra back to its original position (B emission remains unaffected).

We found that oleic acid treatment of pristine WS_2 samples did not significantly improve PL emission, unlike previous reports. We attribute this to oxygen atoms occupying sulfur

vacancies, removing in-gap states and preventing oleic acid from binding to or reacting with them. This suggests that oleic acid’s presence alone does not enhance PL emission, contradicting a purely physical interaction mechanism as, e.g., charge transfer resulting in reduced trion formation. We suggest that PL recovery is due to oxygen atoms provided indirectly during oleic acid treatment, which saturate V_S sites. This mechanism is supported by the fact that only point defects, not larger defects (see SI), can be healed.

While O_2 molecules might be present on the surface, they do not dissociate readily at V_S .^{38,56} Therefore, another source for oxygen must be involved. To support our claim, that the oleic acid provides the oxygen, we performed DFT calculations on the reduction of oleic acid to a fatty aldehyde, releasing an oxygen atom. Figures 5b) and 5c) display the calculated minimum energy path for the reduction of oleic acid and deprotonated oleic acid at V_S , respectively. While the former reaction is found to be endothermic by 0.22 eV, the latter is exothermic by 0.19 eV. As shown in Figure 5b), oleic acid reduction proceeds by elongation of the bond between the hydroxy group and the acyl head, with an energy barrier of 2.37 eV. The reduction of deprotonated oleic acid is more likely, see Figure 5c): After breaking the carbon-oxygen bond, the oxygen atom inserts itself into the sulfur vacancy, with an energy barrier of 1.54 eV. We note that thermal activation suffices to overcome the barrier of 1.54 eV even at room temperature. Eventually, we verified that for both reactions, the in-gap states associated with V_S are indeed removed. This is concluded from Figures 5e) and f), showing the calculated density of states in the final state of the reactions.

Supplementary DFT calculations have been carried out to address the transfer of a hydrogen atom from oleic acid to the sulfur vacancy. These studies are relevant since alternative passivation strategies using super-acids⁵⁷ such as TFMS⁵⁸ or TFSI²⁹⁻³¹ point to the role of hydrogen transfer for enhancing PL yield. Here we note that oleic acid is known to be a weak acid (pKa 9.85⁵⁹), making hydrogen transfer *a priori* less likely in this case. Thus, different mechanisms are likely to be at work in super-acids as compared to oleic acid. In line with this observation, our own DFT calculations (see SI) show that oleic acid, both in its integral

or deprotonated form, can adsorb either on-top of or inside the sulfur vacancy, but in all four geometries studied by us, the passivation of the dangling bonds was incomplete. However, deprotonation at V_S could still play a role as a first step followed by reduction to the fatty aldehyde, as described above. We note that other chemicals, in particular sulfur-containing ones,⁶⁰ e.g. thiols,⁶¹ may provide an alternative route to PL recovery, as has been discussed in the literature.

In summary, we systematically investigated the impact of thermally induced vacancies on A and B emission through *in-situ* measurements. We observed a strong effect on A excitons, while B excitons were almost unaffected by vacancy-induced defect states, suggesting that the correlation between the two excitonic signals is defect-type dependent. The energetic difference between A and B emission is influenced by the defect density. Our results demonstrate oleic acid’s effectiveness in restoring the material’s optoelectronic properties. We showed that oleic acid primarily saturates existing sulfur vacancies. Our calculations indicate that the PL enhancement observed with oleic acid is primarily due to the introduction of substitutional oxygen, which heals vacancies and removes in-gap states. No further significant improvement beyond oxygen substitution could be achieved.

Methods

Sample Preparation

WS_2 samples were grown via chemical vapor deposition (CVD) on SiO_2/Si substrates. To prepare the growth substrates, an aqueous solution was mixed from 3.2 mL of ammonium metatungstate (AMT, Sigma Aldrich), 2 mL of OptiPrep (Sigma Aldrich), and 0.8 mL of DI water. This solution was spin-coated onto p-doped Si substrates with a 285 nm SiO_2 layer,⁶² followed by spin-coating cholic acid sodium salt (Sigma Aldrich) and subsequent annealing at 500°C for 45 minutes to convert AMT to WO_3 .

The CVD growth was performed in a three-zone tube furnace with a quartz tube (Therm-

Concept) connected to an Ar source and exhaust, providing a flow rate of 500 sccm. The first zone was heated to 170 °C with 350 mg of sulfur (S powder, Sigma Aldrich, 99.98%), while the growth substrates were positioned in the second zone at 725 °C for 60 minutes to form WS₂. The third zone was kept at 600 °C to remove reaction by-products.

Using transfer-free samples eliminates defects formed during transfer processes, such as localized strain caused by impurities on intermediate surfaces.⁶³

Thermal Treatment

The sample was placed in a Linkam THMS350V vacuum chamber, achieving a medium vacuum of $5 \cdot 10^{-3}$ mbar. It was heated to various temperatures (up to 623 K) for 30 minutes, then rapidly cooled to 80 K using liquid nitrogen. PL measurements were taken at 80 K once equilibrium was reached.

PL Measurements

PL measurements were performed using a Witec Alpha300 R setup. Spectra were averaged from 10 measurements with a 457 nm laser, focused to ≈ 830 nm spatial resolution. The full spectrum (1.5-2.7 eV) was taken to normalize the signal after background subtraction, using the Si substrate's secondary Raman mode (985 cm^{-1}). A constant laser power of $1.25 \times 10^5 \text{ W/cm}^2$ was used, with the laser spot readjusted and refocused for each measurement to minimize signal fluctuations. All measurements were conducted at 80 K under vacuum conditions.

Oleic Acid Post-Treatment

We followed Tanoh et al.'s instructions³³ for oleic acid treatment. After heating, the sample was transferred to a nitrogen-filled glovebox and placed on a heating plate kept at 25 °C. Degassed oleic acid was carefully dropped onto the sample, covering the substrate. After 16

hours, the oleic acid was washed away with toluene and dried with nitrogen.

DFT Calculations

First-principles calculations were performed using Density Functional Theory (DFT) with VASP 6.3.0 version package.^{64,65} The interactions between ions and valence electrons were described using the projector-augmented wave (PAW)⁶⁶ method, and electronic exchange and correlation were treated by the generalized gradient approximation of Perdew, Burke, and Ernzerhof (PBE).⁶⁷ We employed a plane wave cut-off energy of 500 eV with an additional correction to the van der Waals dispersion interaction in the form of Becke-Johnson damping function D3.⁶⁸ The material models including the defected system were built in a $6 \times 6 \times 1$ supercell with 15 Å vacuum to avoid interaction with the periodic images, which corresponds to a defect density of $2.1 \times 10^{13} \text{ cm}^{-2}$. A $9 \times 9 \times 1$ Monkhorst-Pack k-point grid was used to sample the 2D Brillouin zone. The unfolding of the band structure was computed using the VASPKIT code.⁶⁹ We constructed the minimum energy path of our reactions using the Nudged Elastic Band (NEB) method.⁷⁰

Large Language Models

We used an LLM (Meta Llama 3.1 8B Instruct) to improve the linguistic quality of the manuscript. Neither this nor any other LLM was used to generate scientific content.

Author Contributions

M.S. and P.K. conceived and supervised the project. L.D. designed the experimental research strategy and performed the measurements. D.S. conducted the theoretical calculations. O.K. fabricated the samples. O.K. and C.L. assisted with performing the measurements. The manuscript was written through contributions of all authors. All authors have given approval to the final version of the manuscript.

Notes

The authors declare no competing financial interest.

Acknowledgement

This work was funded by the Deutsche Forschungsgemeinschaft (DFG, German Research Foundation) - project numbers 461605777 (IRTG 2803 2D MATURE) and 429784087. The authors acknowledge support by technical staff, especially Anke Hierzenberger, and helpful discussions with German Sciani. The authors gratefully acknowledge the computing time granted by the Center for Computational Sciences and Simulation (CCSS) of the University of Duisburg-Essen and provided on the supercomputer magnitUDE (DFG Grant No. INST 20876/209-1 FUGG and INST 20876/243-1 FUGG) at the Zentrum für Informations und Mediendienste (ZIM).

References

- (1) Mak, K. F.; Lee, C.; Hone, J.; Shan, J.; Heinz, T. F. Atomically thin MoS₂: a new direct-gap semiconductor. *Physical Review Letters* **2010**, *105*, 136805.
- (2) Gutiérrez, H. R.; Perea-López, N.; Elías, A. L.; Berkdemir, A.; Wang, B.; Lv, R.; López-Urías, F.; Crespi, V. H.; Terrones, H.; Terrones, M. Extraordinary room-temperature photoluminescence in triangular WS₂ monolayers. *Nano Letters* **2013**, *13*, 3447–3454.
- (3) Chernikov, A.; Berkelbach, T. C.; Hill, H. M.; Rigosi, A.; Li, Y.; Aslan, O. B.; Reichman, D. R.; Hybertsen, M. S.; Heinz, T. F. Exciton binding energy and nonhydrogenic Rydberg series in monolayer WS₂. *Physical Review Letters* **2014**, *113*, 076802.
- (4) Gusakova, J.; Wang, X.; Shiao, L. L.; Krivosheeva, A.; Shaposhnikov, V.; Borisenko, V.; Gusakov, V.; Tay, B. K. Electronic Properties of Bulk and Monolayer TMDs: Theoret-

- ical Study Within DFT Framework (GVJ-2e Method). *physica status solidi (a)* **2017**, *214*, 1700218.
- (5) Zhu, B.; Chen, X.; Cui, X. Exciton binding energy of monolayer WS₂. *Scientific Reports* **2015**, *5*, 9218.
- (6) Zeng, H.; Liu, G.-B.; Dai, J.; Yan, Y.; Zhu, B.; He, R.; Xie, L.; Xu, S.; Chen, X.; Yao, W.; Cui, X. Optical signature of symmetry variations and spin-valley coupling in atomically thin tungsten dichalcogenides. *Scientific Reports* **2013**, *3*, 1608.
- (7) Zhao, W.; Ghorannevis, Z.; Chu, L.; Toh, M.; Kloc, C.; Tan, P.-H.; Eda, G. Evolution of electronic structure in atomically thin sheets of WS₂ and WSe₂. *ACS nano* **2013**, *7*, 791–797.
- (8) Xin, X.; Zhang, Y.; Chen, J.; Chen, M.-L.; Xin, W.; Ding, M.; Bao, Y.; Liu, W.; Xu, H.; Liu, Y. Defect-suppressed submillimeter-scale WS₂ single crystals with high photoluminescence quantum yields by alternate-growth-etching CVD. *Materials Horizons* **2022**, *9*, 2416–2424.
- (9) Lee, Y.; Forte, J. D. S.; Chaves, A.; Kumar, A.; Tran, T. T.; Kim, Y.; Roy, S.; Taniguchi, T.; Watanabe, K.; Chernikov, A.; Jang, J. I.; Low, T.; Kim, J. Boosting quantum yields in two-dimensional semiconductors via proximal metal plates. *Nature Communications* **2021**, *12*, 7095.
- (10) Kim, H.; Uddin, S. Z.; Higashitarumizu, N.; Rabani, E.; Javey, A. Inhibited nonradiative decay at all exciton densities in monolayer semiconductors. *Science (New York, N. Y.)* **2021**, *373*, 448–452.
- (11) Andrzejewski, D.; Oliver, R.; Beckmann, Y.; Grundmann, A.; Heuken, M.; Kalisch, H.; Vescan, A.; Kümmell, T.; Bacher, G. Flexible Large-Area Light-Emitting Devices Based on WS₂ Monolayers. *Advanced Optical Materials* **2020**, *8*, 2000694.

- (12) Hutten, U.; Daniel, L.; Grundmann, A.; Stracke, N.; Abdelbaky, M.; Beckmann, Y.; Heuken, M.; Mertin, W.; Kalisch, H.; Vescan, A.; Bacher, G.; Kümmell, T. Transfer-free, scalable photodetectors based on MOCVD-grown 2D-heterostructures. *2D Materials* **2021**, *8*, 045015.
- (13) Bertolazzi, S.; Bonacchi, S.; Nan, G.; Pershin, A.; Beljonne, D.; Samorì, P. Engineering Chemically Active Defects in Monolayer MoS₂ Transistors via Ion-Beam Irradiation and Their Healing via Vapor Deposition of Alkanethiols. *Advanced Materials* **2017**, *29*, 1606760.
- (14) Liu, H.; Wang, C.; Zuo, Z.; Liu, D.; Luo, J. Direct Visualization of Exciton Transport in Defective Few-Layer WS₂ by Ultrafast Microscopy. *Advanced Materials* **2020**, *32*, e1906540.
- (15) Sleziona, S.; Kharsah, O.; Skopinski, L.; Daniel, L.; Schmeink, J.; Schleberger, M. Influence of Highly Charged Ion Irradiation on the Electrical and Memory Properties of Black Phosphorus Field-Effect Transistors. *Advanced Electronic Materials* **2024**, *n/a*, 2400318.
- (16) Pollmann, E.; Madauß, L.; Schumacher, S.; Kumar, U.; Heuvel, F.; vom Ende, C.; Yilmaz, S.; Güngörmüs, S.; Schleberger, M. Apparent differences between single layer molybdenum disulphide fabricated via chemical vapour deposition and exfoliation. *Nanotechnology* **2020**, *31*, 505604.
- (17) Bianchi, M. G.; Risplendi, F.; Re Fiorentin, M.; Cicero, G. Engineering the Electrical and Optical Properties of WS₂ Monolayers via Defect Control. *Advanced Science* **2024**, *11*, e2305162.
- (18) Sleziona, S.; Pelella, A.; Faella, E.; Kharsah, O.; Skopinski, L.; Maas, A.; Liebsch, Y.; Schmeink, J.; Bartolomeo, A. D.; Schleberger, M. Manipulation of the electrical and

- memory properties of MoS₂ field-effect transistors by highly charged ion irradiation. *Nanoscale Adv.* **2019**, *5*, 6958.
- (19) Pelella, A.; Kharsah, O.; Grillo, A.; Urban, F.; Passacantando, M.; Giubileo, F.; Iemmo, L.; Sleziona, S.; Pollmann, E.; Madauß, L.; Schleberger, M.; Di Bartolomeo, A. Electron Irradiation of Metal Contacts in Monolayer MoS₂ Field-Effect Transistors. *ACS Applied Materials & Interfaces* **2020**, *12*, 40532–40540.
- (20) Li, W.-F.; Fang, C.; van Huis, M. A. Strong spin-orbit splitting and magnetism of point defect states in monolayer WS₂. *Physical Review B* **2016**, *94*, 195425.
- (21) Wang, Y.-H.; Ho, H.-M.; Ho, X.-L.; Lu, L.-S.; Hsieh, S.-H.; Huang, S.-D.; Chiu, H.-C.; Chen, C.-H.; Chang, W.-H.; White, J. D.; Tang, Y.-H.; Woon, W.-Y. Photoluminescence Enhancement in WS₂ Nanosheets Passivated with Oxygen Ions: Implications for Selective Area Doping. *ACS Applied Nano Materials* **2021**, *4*, 11693–11699.
- (22) Cui, Q.; Luo, Z.; Cui, Q.; Zhu, W.; Shou, H.; Wu, C.; Liu, Z.; Lin, Y.; Zhang, P.; Wei, S.; Yang, H.; Chen, S.; Pan, A.; Song, L. Robust and High Photoluminescence in WS₂ Monolayer through In Situ Defect Engineering. *Advanced Functional Materials* **2021**, *31*, 2105339.
- (23) Hopster, J.; Kozubek, R.; Krämer, J.; Sokolovsky, V.; Schleberger, M. Ultra-thin MoS₂ irradiated with highly charged ions. *Nucl. Instr. Meth. B* **2013**, *317*, 165.
- (24) Madauß, L.; Ochedowski, O.; Lebius, H.; Ban-d'Etat, B.; Naylor, C.; Johnson, A.; Kotakoski, J.; Schleberger, M. Defect engineering of single- and few-layer MoS₂ by swift heavy ion irradiation 2D Materials. *2D Materials* **2017**, *4*, 015034.
- (25) Schleberger, M.; Kotakoski, J. 2D Material Science: Defect Engineering by Particle Irradiation. *Materials* **2018**, *11*, 1885.

- (26) Kozubek, R.; Tripathi, M.; Ghorbani-Asl, M.; Kretschmer, S.; Madauß, L.; Pollmann, E.; O’Brien, M.; McEvoy, N.; Ludacka, U.; Susi, T.; Duesberg, G.; Wilhelm, R.; Krashenninnikov, A.; Kotakoski, J.; Schleberger, M. Perforationg Freestanding Molybdenum Disulfide Monolayers with Highly Charged Ions. *J. Phys. Chem. Lett.* **2019**, *10*, 904.
- (27) Mitterreiter, E. et al. The role of chalcogen vacancies for atomic defect emission in MoS₂. *Nature Communications* **2021**, *12*, 3822.
- (28) Asaithambi, A.; Kozubek, R.; Prinz, G. M.; Reale, F.; Pollmann, E.; Ney, M.; Mattevi, C.; Schleberger, M.; Lorke, A. Laser- and Ion-Induced Defect Engineering in WS₂ Monolayers. *physica status solidi (RRL) – Rapid Research Letters* **2021**, *15*, 2000466.
- (29) Kiriya, D.; Lien, D.-H. Superacid Treatment on Transition Metal Dichalcogenides. *Nano Express* **2022**, *3*, 034002.
- (30) Amani, M. et al. Near-unity photoluminescence quantum yield in MoS₂. *Science (New York, N.Y.)* **2015**, *350*, 1065–1068.
- (31) Lu, H.; Kummel, A.; Robertson, J. Passivating the sulfur vacancy in monolayer MoS₂. *APL Materials* **2018**, *6*, 066104.
- (32) Cadore, A. R. et al. Monolayer WS₂ electro- and photo-luminescence enhancement by TFSI treatment. *2D Materials* **2024**, *11*, 025017.
- (33) Tanoh, A. O. A.; Alexander-Webber, J.; Xiao, J.; Delport, G.; Williams, C. A.; Bretscher, H.; Gauriot, N.; Allardice, J.; Pandya, R.; Fan, Y.; Li, Z.; Vignolini, S.; Stranks, S. D.; Hofmann, S.; Rao, A. Enhancing Photoluminescence and Mobilities in WS₂ Monolayers with Oleic Acid Ligands. *Nano Letters* **2019**, *19*, 6299–6307.
- (34) Tanoh, A. O. A.; Alexander-Webber, J.; Fan, Y.; Gauriot, N.; Xiao, J.; Pandya, R.;

- Li, Z.; Hofmann, S.; Rao, A. Giant photoluminescence enhancement in MoSe₂ monolayers treated with oleic acid ligands. *Nanoscale Advances* **2021**, *3*, 4216–4225.
- (35) Lin, D.; Ni, W.; Gurzadyan, G. G.; Zhang, F.; Zhao, W.; Ma, L.; Nie, Z. Trap-free exciton dynamics in monolayer WS₂ via oleic acid passivation. *Nanoscale* **2021**, *13*, 20126–20133.
- (36) Wang, Y.; Zhai, X.; Feng, L.; Gao, T. Enhancing excitons by oleic acid treatment in WS₂, MoS₂, and WS₂/MoS₂ heterostructure. *Applied Physics Express* **2022**, *15*, 022005.
- (37) Barja, S. et al. Identifying substitutional oxygen as a prolific point defect in monolayer transition metal dichalcogenides. *Nature Communications* **2019**, *10*, 3382.
- (38) Luo, Z.; Zheng, W.; Luo, N.; Liu, B.; Zheng, B.; Yang, X.; Liang, D.; Qu, J.; Liu, H.; Chen, Y.; Jiang, Y.; Chen, S.; Zou, X.; Pan, A. Photoluminescence Lightening: Extraordinary Oxygen Modulated Dynamics in WS₂ Monolayers. *Nano Letters* **2022**, *22*, 2112–2119.
- (39) Hu, Z.; Avila, J.; Wang, X.; Leong, J. F.; Zhang, Q.; Liu, Y.; Asensio, M. C.; Lu, J.; Carvalho, A.; Sow, C. H.; Castro Neto, A. H. The Role of Oxygen Atoms on Excitons at the Edges of Monolayer WS₂. *Nano Letters* **2019**, *19*, 4641–4650.
- (40) Berkdemir, A.; Gutiérrez, H. R.; Botello-Méndez, A. R.; Perea-López, N.; Elías, A. L.; Chia, C.-I.; Wang, B.; Crespi, V. H.; López-Urías, F.; Charlier, J.-C.; Terrones, H.; Terrones, M. Identification of individual and few layers of WS₂ using Raman Spectroscopy. *Scientific Reports* **2013**, *3*, 1–8.
- (41) Zhao, W.; Ghorannevis, Z.; Amara, K. K.; Pang, J. R.; Toh, M.; Zhang, X.; Kloc, C.; Tan, P. H.; Eda, G. Lattice dynamics in mono- and few-layer sheets of WS₂ and WSe₂. *Nanoscale* **2013**, *5*, 9677–9683.

- (42) Staiger, M.; Gillen, R.; Scheuschner, N.; Ochedowski, O.; Kampmann, F.; Schleberger, M.; Thomsen, C.; Maultzsch, J. Splitting of the monolayer out-of-plane A₁ Raman mode in few-layer WS₂. *Phys. Rev. B* **2015**, *91*, 195419.
- (43) Christopher, J. W.; Goldberg, B. B.; Swan, A. K. Long tailed trions in monolayer MoS₂: Temperature dependent asymmetry and resulting red-shift of trion photoluminescence spectra. *Scientific Reports* **2017**, *7*, 14062.
- (44) McCreary, K. M.; Hanbicki, A. T.; Sivaram, S. V.; Jonker, B. T. A- and B-exciton photoluminescence intensity ratio as a measure of sample quality for transition metal dichalcogenide monolayers. *APL Materials* **2018**, *6*, 111106.
- (45) Lu, W.; Birmingham, B.; Zhang, Z. Defect engineering on MoS₂ surface with argon ion bombardments and thermal annealing. *Applied Surface Science* **2020**, *532*, 147461.
- (46) Ross, J. S.; Wu, S.; Yu, H.; Ghimire, N. J.; Jones, A. M.; Aivazian, G.; Yan, J.; Mandrus, D. G.; Di Xiao; Yao, W.; Xu, X. Electrical control of neutral and charged excitons in a monolayer semiconductor. *Nature Communications* **2013**, *4*, 1474.
- (47) Mouri, S.; Miyauchi, Y.; Matsuda, K. Tunable photoluminescence of monolayer MoS₂ via chemical doping. *Nano Letters* **2013**, *13*, 5944–5948.
- (48) Li, Y.; Li, X.; Chen, H.; Shi, J.; Shang, Q.; Zhang, S.; Qiu, X.; Liu, Z.; Zhang, Q.; Xu, H.; Liu, W.; Liu, X.; Liu, Y. Controlled Gas Molecules Doping of Monolayer MoS₂ via Atomic-Layer-Deposited Al₂O₃ Films. *ACS Applied Materials & Interfaces* **2017**, *9*, 27402–27408.
- (49) Hichri, A.; Ben Amara, I.; Ayari, S.; Jaziri, S. Exciton center-of-mass localization and dielectric environment effect in monolayer WS₂. *Journal of Applied Physics* **2017**, *121*.
- (50) Gaur, A. P. S.; Rivera, A. M.; Dash, S. P.; Dey, S.; Katiyar, R. S.; Sahoo, S. Manipula-

- tion of exciton and trion quasiparticles in monolayer WS₂ via charge transfer. *Applied Physics Letters* **2019**, *115*.
- (51) Zhang, X.; Gao, L.; Yu, H.; Liao, Q.; Kang, Z.; Zhang, Z.; Zhang, Y. Single-Atom Vacancy Doping in Two-Dimensional Transition Metal Dichalcogenides. *Accounts of Materials Research* **2021**, *2*, 655–668.
- (52) Shen, P.-C. et al. Healing of donor defect states in monolayer molybdenum disulfide using oxygen-incorporated chemical vapour deposition. *Nature Electronics* **2022**, *5*, 28–36.
- (53) Wang, G.; Robert, C.; Suslu, A.; Chen, B.; Yang, S.; Alamdari, S.; Gerber, I. C.; Amand, T.; Marie, X.; Tongay, S.; Urbaszek, B. Spin-orbit engineering in transition metal dichalcogenide alloy monolayers. *Nature Communications* **2015**, *6*, 10110.
- (54) Rigosi, A. F.; Hill, H. M.; Rim, K. T.; Flynn, G. W.; Heinz, T. F. Electronic band gaps and exciton binding energies in monolayer MoxW_{1-x}S₂ transition metal dichalcogenide alloys probed by scanning tunneling and optical spectroscopy. *Physical Review B* **2016**, *94*, 075440.
- (55) Schuler, B.; Qiu, D. Y.; Refaely-Abramson, S.; Kastl, C.; Chen, C. T.; Barja, S.; Koch, R. J.; Ogletree, D. F.; Aloni, S.; Schwartzberg, A. M.; Neaton, J. B.; Louie, S. G.; Weber-Bargioni, A. Large Spin-Orbit Splitting of Deep In-Gap Defect States of Engineered Sulfur Vacancies in Monolayer WS₂. *Physical Review Letters* **2019**, *123*, 076801.
- (56) Bianchi, M.; Risplendi, F.; Re Fiorentin, M.; Cicero, G. Addressing the effects of gas adsorption on monolayers beyond charge population analysis: the case of WS₂. *npj Comput. Mater.* **2024**, *10*, 62.
- (57) Yamada, Y.; Shinokita, K.; Okajima, Y.; Takeda, S. N.; Matsushita, Y.; Takei, K.; Yoshimura, T.; Ashida, A.; Fujimura, N.; Matsuda, K.; Kiriya, D. Photoactivation

- of Strong Photoluminescence in Superacid-Treated Monolayer Molybdenum Disulfide. *ACS Applied Materials & Interfaces* **2020**, *12*, 36496–36504.
- (58) Feng, Q.; Sun, Y.; Li, Y.; Yan, J.; Zhong, W.; Yang, G.; Liu, W.; Xu, H.; Liu, Y. Highly Photoluminescent Monolayer MoS₂ and WS₂ Achieved via Superacid Assisted Vacancy Reparation and Doping Strategy. *Laser & Photonics Reviews* **2021**, *15*, 2100104.
- (59) Kanicky, J. R.; Shah, D. O. Effect of degree, type, and position of unsaturation on the pK_a of long-chain fatty acids. *Journal of Colloid and Interface Science* **2002**, *256*, 201–207.
- (60) Roy, S.; Choi, W.; Jeon, S.; Kim, D.-H.; Kim, H.; Yun, S. J.; Lee, Y.; Lee, J.; Kim, Y.-M.; Kim, J. Atomic Observation of Filling Vacancies in Monolayer Transition Metal Sulfides by Chemically Sourced Sulfur Atoms. *Nano Letters* **2018**, *18*, 4523–4530.
- (61) Schwarz, A. et al. Thiol-based defect healing of WSe₂ and WS₂. *npj 2D Materials and Applications* **2023**, *7*, 1–9.
- (62) An, G. H.; Jin Kim, S.; Kim, S.; Shin, S. J.; Choi, M.; Kim, D.; Rahman, I. N.; Bang, J.; Kim, K.; Kim, D.-H.; Lee, H. S. Growth mode control of CVD-grown WS₂ monolayer flakes via O₂ pre-annealing for organic surfactant oxidation. *Applied Surface Science* **2022**, *585*, 152564.
- (63) Lee, S.-Y.; Jeong, T.-Y.; Ahn, S.; Jung, S.; Cho, Y.-H.; Yee, K.-J. Effective Photoluminescence Imaging of Bubbles in hBN-Encapsulated WSe₂ Monolayer. *Nanomaterials* **2020**, *10*, 350.
- (64) Kresse, G.; Furthmüller, J. Efficient iterative schemes for ab initio total-energy calculations using a plane-wave basis set. *Physical review. B, Condensed matter* **1996**, *54*, 11169–11186.

- (65) Kresse, G.; Joubert, D. From ultrasoft pseudopotentials to the projector augmented-wave method. *Physical review. B, Condensed matter* **1999**, *59*, 1758–1775.
- (66) Blöchl, P. E. Projector augmented-wave method. *Physical review. B, Condensed matter* **1994**, *50*, 17953–17979.
- (67) Perdew, J. P.; Burke, K.; Ernzerhof, M. Generalized Gradient Approximation Made Simple. *Physical Review Letters* **1996**, *77*, 3865–3868.
- (68) Grimme, S.; Ehrlich, S.; Goerigk, L. Effect of the damping function in dispersion corrected density functional theory. *Journal of Computational Chemistry* **2011**, *32*, 1456–1465.
- (69) Wang, V.; Xu, N.; Liu, J.-C.; Tang, G.; Geng, W.-T. VASPKIT: A user-friendly interface facilitating high-throughput computing and analysis using VASP code. *Computer Physics Communications* **2021**, *267*, 108033.
- (70) Henkelman, G.; Uberuaga, B. P.; Jónsson, H. A climbing image nudged elastic band method for finding saddle points and minimum energy paths. *The Journal of Chemical Physics* **2000**, *113*, 9901–9904.

TOC Graphic

